Guest/Host Relationships in the Synthesis of the Novel Cage-Based Zeolites SSZ-35, SSZ-36, and SSZ-39

Paul Wagner,[†] Yumi Nakagawa,[‡,§] Greg S. Lee,[⊥,‡] Mark E. Davis,[†] Saleh Elomari,[‡] Ronald C. Medrud,[‡] and S. I. Zones*,[‡]

Contribution from the California Institute of Technology, Pasedena, California 91125, and Chevron Research and Technology Company, Richmond, California 94802

Received March 5, 1999. Revised Manuscript Received August 12, 1999

Abstract: Here, we report the synthesis and structure of three high-silica molecular sieves, SSZ-35, SSZ-36, and SSZ-39, that are prepared from a library of 37 different cyclic and polycyclic quaternized amine molecules that are used as structure-directing agents (SDAs). The size and shape of the quaternized amine molecules are purposely designed in order to obtain novel zeolite structures, and the synthesis of these molecules is presented. The selectivity for the three molecular sieve phases is found to depend on both the SDA and the degree of heteroatom lattice substitution of Al^{3+} or B^{3+} in the silicate framework. Molecular modeling is utilized to probe the effects of the nonbonded SDA/zeolite-framework interaction energy on the selectivity for the observed molecular sieve phase. The Rietveld refinement of the powder X-ray data confirms the structure of the SSZ-39 zeolite to be isomorphous with the aluminophosphate molecular sieve, SAPO-18 (AEI). The structure of SSZ-36 is found to possess a range of fault probabilities between the two-dimensional channel system, end-member polymorphs, ITQ-3 and RUB-13 (International Zeolite Association Codes ITE and RTH, respectively). The SSZ-35 structure is reported to contain a one-dimensional pore system possessing stacked cages circumscribed by alternating rings of 10 and 18 tetrahedral atoms (10- and 18-membered rings).

Introduction

There remains a keen interest in developing new, three-dimensional, zeolitic silicate frameworks, as these materials have found commercial use in hydrocarbon processing. Catalysts based upon zeolites continue to proliferate in the extent of varied uses in the modern refinery.[1] New zeolite structures lend themselves to the possibility of finding niches in processing based upon shape-selective capabilities. This trend represents a step change from much of the previous applications of Y zeolites (FAU) that perform most of the large-scale catalyst work in areas such as FCC and hydrocracking. Recent examples where niche selectivities of zeolites have been exploited are in the replacement of solvent extraction by shape-selective zeolites capable of isomerization dewaxing[2] in the pursuit of high-quality lube oil base stocks and the introduction of zeolitic catalysts to replace phosphoric acid on a silica support in the production of cumene from benzene and propylene.[3] Cumene is then oxidized in a commercial process to produce both phenol and acetone.

Many of the novel silica-based zeolite structures are derived from the use of organocations as guest molecules in the crystallizing product; i.e., they effectively stabilize the void regions within the inorganic structure. A popularization of this guest activity has been to refer to them as "template" molecules[4]

or as "structure-directing agents" (SDAs).[5] Clearly, part of the challenge in synthesizing new zeolites is to develop candidate guest molecules that have the potential to generate novel zeolite structures. While the size and shape of the guest molecules often correlate well with the void dimensions within the host, there are still aspects of phase selectivity in zeolite synthesis that are kinetically controlled. That is, the same organocation guest may be capable of crystallizing more than one zeolitic phase.[6] Thus, while research becomes ever more sophisticated in molecular modeling approaches toward developing favorable guest/host interactions,[7] the experimentalist is still faced with the question of what controls "how to get there".[8]

From the standpoint of empirical learning, we have divided the field of high-silica zeolite formation into five domains that are related by the extent of lattice substitution and the size of the guest SDA molecule. With small SDA molecules and little heteroatom lattice substitution, clathrates are the favored product.[9] Clathrates are cage-based structures in which the guest molecule is surrounded by an inorganic lattice with portals too small to allow any communication between cages. As the guest molecules become larger, the second domain is observed in which one-dimensional, parallel pore systems are found at the

---

[†] California Institute of Technology.

[‡] Chevron Research and Technology Co.

[§] Current address: Chiron Technologies, Emeryville, California.

[⊥] Current address: Lawrence Livermore National Laboratory, Livermore, California.

(1) Absi-Halabi, A.; Stanislaus, A.; Qabazard, H. *Hydrocarbon Processing* **1997**, *Feb*, 45.

(2) Miller, S. J. Wax Isomerization for Improved Lube Oil Quality. Presented at the AIChE Spring Meeting, New Orleans, LA, March, 1998 (see abstracts).

(3) Innes, R. A.; Nacamuli, G.; Zones, S. I. U.S. Patent 4,891,458, 1990.

(4) Lok, B. M.; Cannan, T. R.; Messina, C. A. *Zeolites* **1983**, *3*, 282.

(5) Lobo, R. F.; Zones, S. I.; Davis, M. E. In *Inclusion Chemistry With Zeolites, Nanoscale Materials by Design*; Herron, N., Corbin, D., Eds.; Kluwer Academic Publishers: Dordrecht, The Netherlands, 1995; Vol. 21, pp 47−78.

(6) Wagner, P.; Yoshikawa, M.; Lovallo, M.; Tsuji, K.; Tsapatsis, M.; Davis, M. E. *J. Chem. Soc., Chem. Commun.* **1997**, 2179−80.

(7) Lewis, D. W.; Willock, D. J.; Catlow, C. R. A.; Thomas, J. M.; Hutchings, G. J. *Nature* **1996**, *382*, p 604.

(8) Davis, M. E.; Zones, S. I. In *Synthesis of Porous Materials*; Occelli, M. L., Kessler, H., Eds.; Marcel Dekker: New York, 1997; p 1.

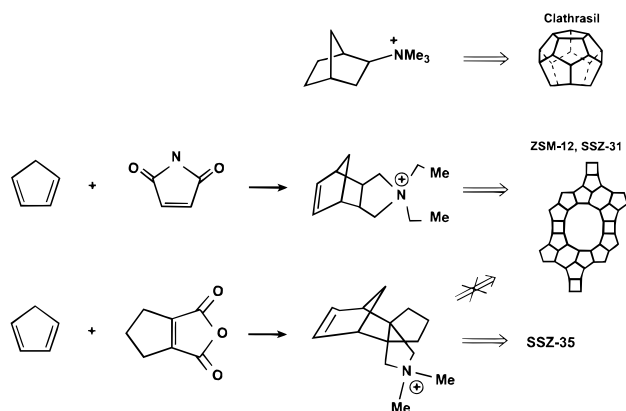(9) Gies, H. *Inclusion Compounds*; Academic Press: London, 1991; Vol. 5, pp 1−35.

Figure 1. Three guest molecules based upon extensions of the Diels−Alder reaction and the types of zeolites generated as spatial features change. (a) The norbornyl derivative is still small enough to generate cage-centered clathrate structures such as nonasil (NON). (b) The tricyclic derivatives with long, central axes produce one-dimensional, large-pore zeolites. ZSM-12 (MTW structure) and SSZ-31 are two different examples of this type of product. (c) The pseudo-propellane developed in this guest leads away from one-dimensional larg-pore zeolites and generates zeolites with cavities such as SSZ-35.

high-silica lattice content. A third case results as lattice substitution increases, and multidimensional channel systems possessing larger overall micropore volumes predominate. A fourth domain is often observed at high lattice substitution, in which the highly heteroatom-substituted zeolites contain cages with smaller portals. The fifth domain arises from the use of large guest molecules with strong nonbonded SDA/zeolite interaction energy resulting in the stabilization of open-framework zeolite lattices; in this case, due to the strong interaction energy, the stabilized framework structure is formed over the entire heteroatom lattice substitution range. The recent report of a pure-phase MEL zeolite (ZSM-11) is an example of this fifth case.[10]

To overcome the propensity for SDA molecules to form clathrate structures, Nakagawa developed a designed organic system that was based upon bringing together individual ring structures in a Diels−Alder reaction to build candidate molecules leading to large-pore zeolites.[11] The individual rings themselves, if converted into charged ammonium compounds, would generate clathrate products. Figure 1 shows three different sized norbornane derivatives (based upon Diels−Alder chemistry) and the transition from clathrate to open-pore structure. Many of the rigid, elongated SDA derivatives formed from variations of cyclopentadiene reacting with maleimides produce open-pore, one-dimensional zeolites such as MTW or SSZ-31 (shown in Figure 1). These two 12-ring zeolites possess different configurations of the pore opening, with MTW containing a somewhat puckered pore opening[12] while SSZ-31 possesses a very open but highly elliptical pore opening with dimensions ranging from 8.8 to 5.5 Å.[13]

(10) (a) Nakagawa, Y. WO 95/09812. (b) Terasaki, O.; Ohsuna, T.; Sakuma, H.; Watanabe, D.; Nakagawa, Y.; Medrud, R. C. *Chem. Mater.* **1996**, *8*, 463. (c) Nijo, S. L.; Koegler, J. H.; van Koningsveld, H.; van de Graaf, B. *Microporous Mater.* **1997**, *8*, 223−230.

(11) Nakagawa, Y.; Zones, S. I. In *Molecular Sieves*; Occelli, M. L., Robson, H. E., Eds.; Van Nostrand Reinhold: New York, 1992; Vol. 1, p 222.

(12) La Pierre, R. B.; Rohrman, A. C., Jr.; Schlenker, J. L.; Wood, J. D.; Rubin, M. K.; Rohrbaugh, W. J. *Zeolites* **1985**, *5*, 346.

(13) (a) Lobo, R. F.; Tsapatsis, M.; Freyhardt, C. C.; Chan, I. Y.; Chen, C. Y.; Zones, S. I.; Davis, M. E. *J. Am. Chem. Soc.* **1997**, *119*, 3732. (b) See: Treacy, M. M. J.; Deem, M. W.; Newsam, J. M. DIFFaX Version 1.801, 1995.

Table 1. Substituted Monocyclic Quaternary Ammonium Templates[a]

Entry #	Structure
1	(Mixture of the Two)
2	
3	
4	
5	
6	
7	
8	

[a] Includes spirocyclic derivative **8** and **9**.

Here, we describe our efforts to synthesize novel zeolite structures by designing SDA molecules that both are too large to fit into the cages of the clathrate-type silicates and possess a spheroidal shape that precludes the formation of the straight one-dimensional channel systems of zeolite structures that tend to form when using rigid elongated SDA molecules, e.g., those of Figure 1b. The initial success of this SDA design effort resulted from a derivative of the camphor-type molecule (entry **9**, Table 2) that led to the crystallization of the novel, open-framework zeolites SSZ-35 and -36. Subsequently, numerous other zeolite structure-directing molecules were discovered using this design strategy (Tables 1−3), and we present a detailed investigation into the guest/host relationship between these organic SDA molecules and the resulting zeolite phases.

Experimental Section

Synthesis of Organocation Structure-Directing Agents (SDAs). The syntheses of the 37 organocation SDAs that appear in Tables 1−3 are reported in the Supporting Information. Table 1 shows the monocyclic organic directing molecules, Table 2 lists the bicyclic organic directing molecules, and Table 3 presents the tri- and tetracyclic organic directing molecules used in this study. The quaternary ammonium guest molecules are used in their hydroxide form after ion-exchanging the halide anion using Bio-Rad AG 1-X8 ion-exchange resin. All reagents are from Aldrich Chemical Co. unless otherwise stated.

Table 2. Substituted Bicyclic Quaternary Ammonium Templates

Entry #	Structure	Entry #	Structure
9		19	
10		20	
11		21	
12		22	
13		23	
14		24	
15		25	
16		26	
17		27	
18			

Zeolite Syntheses. The individual zeolite synthesis reactions are run in Parr reactors of 23-mL capacity. The crystalline products are generally collected on glass frits, washed with roughly 100 times the amount of water as the initial reaction solution, and then air-dried before XRD patterns are obtained on a Siemens D-500 instrument. The six different zeolite syntheses run for the majority of the 37 guest molecules reported here were recently described,[14] and a representative procedure for each synthesis is presented. The reactions are labeled as to starting silica-to-alumina ratio (SAR) or, in one case, the corresponding ratio for silica and borate. These reactions correspond to the entries found in Table 4, in which the reaction product is presented.

SAR = 30: 2 mmol of the guest molecule hydroxide is mixed with 0.20 g of 1 N NaOH and the mass brought to 6 g with water. Then, 2.5 g of Banco "N" silicate is added (28 wt % SiO_2, 8.9 wt % Na_2O). Also, 0.25 g of Union Carbide's LZY-62 (25% H_2O) is added as an aluminum source. The reaction is heated at 135 °C and 43 rpm and is checked every 3−4 days for a pH jump (from near 11.80 to 12.50).

SAR = 40: 2.15 mmol of guest molecule hydroxide is mixed with 1.43 g of 1 N NaOH and the mass brought to 7.2 g with the addition of water. Also, 0.25 g of Union Carbide's LZY-52 (25% H_2O) zeolite is added as aluminum source, and finally 0.80 g of Cabosil-M5 is added. This reaction is run like the one above but at 160 °C.

SAR = 70: 3 mmol of the organic hydroxide is mixed with 0.76 g of 1 N NaOH, and the total mass is brought to 7 g with water. Also, 0.25 g of Union Carbide's LZ 210 (18% H_2O) and 0.74 g of Cabosil-M5 are added, and the reaction is run at 170 °C and 43 rpm.

SAR = 100: 2.15 mmol of organic hydroxide and 1.50 mmol of 1 N NaOH are brought up to a mass of 11.75 g with water. Then, 0.03 g of Reheis F-2000 alumina (53 wt % Al_2O_3) is dissolved. Finally, 0.90 g of Cabosil-M5 is blended in, and the reaction is carried out at 170 °C with 43 rpm.

SAR = 300: In this reaction, Tosoh's 390 HUA is used as the Si and Al source.[15] First, 2.25 mmol of organic hydroxide and 2.25 mmol of 1 N NaOH are combined, and the mass is brought to 10 g with water. Then, 0.90 g of Tosoh 390 HUA is added, and the reaction is heated at 160 °C with 43 rpm tumbling.

SiO_2/B_2O_3 = 30: 2.25 mmol of organic hydroxide in 4.35 mL of water is used to dissolve 0.095 g of sodium borate decahydrate. When the solution is clear, 1.36 g of Dupont's Ludox AS-30 (30% SiO_2) is added, and the reaction is heated at 160 °C without stirring. The

(14) Nakagawa, Y.; Lee, G. S.; Harris, T. V.; Yuen, L. T.; Zones, S. I. *Microporous Mesoporous Mater.* **1998**, *22*, 69.

(15) Zones, S. I.; Nakagawa, Y. WO 96/29,284, 1996.

Table 3. Tri- and Tetracyclic Quaternary Ammonium Templates

Entry #	Structure
28	
29	
30	
31	
32	
33	
34	
35	
36	
37	

completion of the reaction is determined by the transformation of the uniform gel into a settled solid.

Sample Preparation for Synchrotron Data Collection. The calcined silicate materials are loaded into 1-mm-diameter glass capillaries, heated to 350 °C under vacuum, and then sealed. The data collected on the X7A synchrotron beamline at the National Synchrotron Light Source at Brookhaven National Laboratory (Upton, NY) are indexed[16] and converted into a format compatible with GSAS[17] for the Rietveld refinement work.

Molecular Modeling. Monte Carlo simulations are conducted at 300 K with a fixed loading of one organic guest molecule per cage.[18] The sorption simulation probes 20 000 guest/host configurations, and the lowest energy result is energy-minimized using the Burchart-Universal force field. The framework atoms are fixed during the energy minimization, and the cationic charge of the organocation is counterbalanced by averaging the negative charge over the framework atoms. The reported stabilization energies represent only the nonbonded van der Waals interactions between the silicate framework and the organic guest.

Results and Discussion

1. Synthesis. Table 4 presents the products that result from each of the 37 structure-directing molecules (Tables 1−3) in

the synthesis reactions with silica-to-alumina ratios (SAR) = 30, 40, 70, 100, and >300 and also with boron lattice substitution (silica-to-borate ratio, SBR = 40). The three-letter code entries in Table 4 are assigned by the International Zeolite Association, and further information on these structures can be found in ref 19. Zeolites that are referred to with an SSZ designation in Table 4 have not yet been assigned structure codes.

a. Observed Zeolite Formation Domains. Entry **2** in Table 4 provides an example of the first domain of zeolite synthesis discussed in the Introduction in which small SDA molecules tend to result in the formation of clathrates at low lattice substitution. The clathrate NON results from the small-molecule SDA, entry **2**, over a range of low lattice substitutions (SAR = 70 → 300), as seen in Table 4. At very low lattice substitution (SAR > 300), the small-molecule SDA, entry **3**, is also seen to direct for the clathrate NON. The results indicate that these small SDA molecules effectively maximize the silica/SDA interaction by stabilizing the small silica cages present in the clathrate materials such as NON and DDR.

As the size of the SDA molecule is increased beyond the small cage size of the clathrates, one-dimensional channel system zeolites tend to form at low lattice substitution. Entry **4**, Table 4 indicates that the *N,N*-diethylpiperidium derivative molecule that possesses a pendent ethyl group off of the carbon ring results in the crystallization of the one-dimensional channel system zeolite SSZ-31 at SAR > 300. Increasing the lattice substitution results in the formation of the multidimensional, 10-membered-ring (MR) zeolite MFI (SAR 40 and 70). This SDA provides examples of the second and third domains of zeolite formation.

At very high lattice substitution, the zeolitic phases denoted SSZ-39 and CHA tend to crystallize from a number of the SDA molecules in Tables 1−3. The most aluminum-rich reaction described in the Experimental Section (SAR = 30) is the best reaction for selectively generating these zeolites. Compared with the other five zeolite synthesis reactions described, the high alumina syntheses also have a much higher OH/Si ratio in the reactants. Zeolite synthesis mixtures containing high alumina and high hydroxide concentrations are favorable for producing cage-based zeolites, such as CHA, with small eight-ring pores and structural subunits constructed of even-membered tetrahedral atom rings.[20] The structure solution of SSZ-39 outlined below also reveals that this zeolite contains cages with eight-ring pores and is composed entirely of four- and six-membered rings of tetrahedral atoms similar to CHA. These even-membered-ring zeolites tend to form at high lattice substitution because the strict alternation of the silicon and aluminum in the framework avoids the energetically unfavorable electrostatic interaction that arises from two adjacently located negatively charged alumina tetrahedra. CHA and SSZ-39 are examples of the fourth zeolite formation domain, in which high-alumina-containing zeolite syntheses result in highly heteroatom-substituted, even-membered-ring-containing zeolites that possess cages with smaller portals.

The tetracyclic Diels−Alder product, entry **29**, Table 3 (also shown in Figure 1c), is an example of a large rigid spheriodal SDA that is designed to obtain novel, open-framework zeolites by avoiding the crystallization of the commonly observed clathrates and straight one-dimensional channel system zeolites.

(16) Werner, P. E.; Erikson, L.; Westdahl, M. J. *J. Appl. Crystallogr.* **1985**, *18*, 367.

(17) Larson, A. C.; Von Dreele, R. B. *GSAS−General Structure Analysis System*; Los Alamos National Laboratory Report, LA-UR 86-748; LANL: Los Alamos, NM, 1986.

(18) *CERIUS 2*, Version 3.5; Molecular Simulations Inc.: Cambridge, UK 1996.

(19) Meier, W. M.; Olson, D. H.; Baerlocher, Ch. *Atlas of Zeolite Structure Types*, 4th ed.; Elseveir: London, 1996.

(20) (a) Zones, S. I.; Van Nordstrand, R. A. *Novel Materials in Heterogeneous Catalysis*; ACS Symposium Series 437; Baker, R. T. K., Murrell, L. L., Eds.; American Chemical Society: Washington, DC, 1990; p 14. (b) Zones, S. I.; van Nordstrand, R. A. *Zeolites* **1989**, *9*, 458.

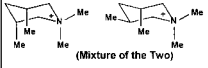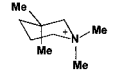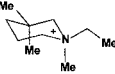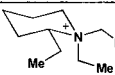**Table 4.** List of Zeolite Reactions and Products
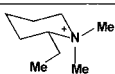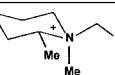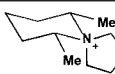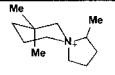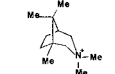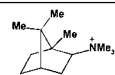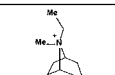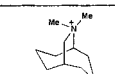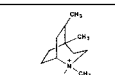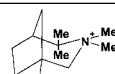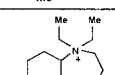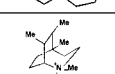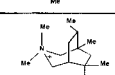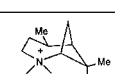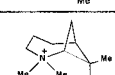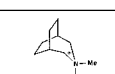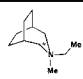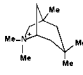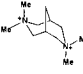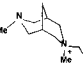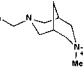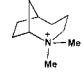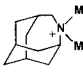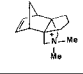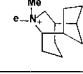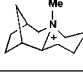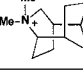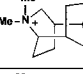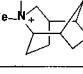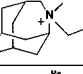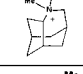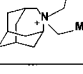
Structure	Entry #	SAR = 30	40	70	100	>300	SiO₂/B₂O₃ = 40
(structure — Mixture of the Two)	1	SSZ-39	MFI	MTW	ZSM-5/11	MTW	SSZ-36
(structure)	2	CHA	CHA	NON	NON	NON	SSZ-36
(structure)	3	CHA	-	EUO	MFI	NON	SSZ-36
(structure)	4	-	MFI	MFI	-	SSZ-31	SSZ-35
(structure)	5	-	MFI	SSZ-31	-	SSZ-31	SSZ-36
(structure)	6	CHA	MFI	MTW	Layer	Layer	SSZ-36
(structure)	7	-	SSZ-35	SSZ-35	SSZ-35	SSZ-31	SSZ-35
(structure)	8	CHA	CHA	CHA	-	Layer	SSZ-33
(structure)	9	SSZ-36	SSZ-35	SSZ-35	SSZ-35	SSZ-35	SSZ-35
(structure)	10		SSZ-36				
(structure)	11	CHA	SSZ-35	SSZ-35	SSZ-35	SSZ-35	SSZ-35
(structure)	12	CHA	CHA/DDR	-	-	DDR	SSZ-35
(structure)	13	-	-	-	-	SGT	SSZ-35
(structure)	14	-	SSZ-35	SSZ-35	SSZ-35	SSZ-35	SSZ-35
(structure)	15	SSZ-36	SSZ-36	SSZ-35	SSZ-35	SSZ-35	SSZ-36
(structure)	16	SSZ-36	-	SSZ-36	SSZ-36	-	-
(structure)	17	SSZ-36	SSZ-36	SSZ-36	SSZ-35	-	SSZ-36
(structure)	18	SSZ-36	SSZ-36	SSZ-36	SSZ-36	-	SSZ-36
(structure)	19	SSZ-36	SSZ-36	SSZ-36	SSZ-36	SSZ-35	SSZ-36
(structure)	20	SSZ-39	SSZ-35	SSZ-35	SSZ-35	SSZ-35	SSZ-35
(structure)	21	MOR	SSZ-28	DDR/SGT	-	DDR	SSZ-35

Table 4.   (Cont'd)

Structure	Entry #	SAR = 30	40	70	100	>300	SiO$_2$/B$_2$O$_3$ = 40
	22	CHA	-	-	-	NON	SSZ-35/CHA
	23	SSZ-39	SSZ-35/36	SSZ-35	-	SSZ-31	SSZ-36
	24	HA/MOR	SSZ-35	SSZ-35	SSZ-35	SSZ-35	SSZ-35
	25	CHA	SSZ-35	SSZ-35	SSZ-35	SSZ-35	SSZ-35
	26	MOR	MFI	MFI	SSZ-35	Layer	-
	27	CHA	DDR	DDR	NON	NON	DDR
	28	CHA	SSZ-35	-	SSZ-35	SSZ-35	SSZ-35
	29	SSZ-35	SSZ-35	-	SSZ-35	SSZ-35	-
	30	SSZ-36	SSZ-35	-	-	SSZ-35	SSZ-35
	31	CHA	SSZ-31	SSZ-31	SSZ-35	SSZ-31	SSZ-35
	32	-	DDR	-	-	DDR	SSZ-35
	33	-	DDR	-	-	DDR/35	SSZ-35
	34	SSZ-35	SSZ-35	-	-	DDR/35	SSZ-35
	35	CHA	SSZ-35	SSZ-24	SSZ-35	-	SSZ-35
	36	CHA	SSZ-35	SSZ-35	SSZ-35	SSZ-35	SSZ-35
	37	CHA	CHA	SSZ-24	SSZ-24	SSZ-24	-

These products result when either small or rigid elongated molecules are employed as SDAs. As can be seen from entry **29** of Table 4, this tetracyclic Diels−Alder SDA molecule is found to have a very high selectivity for the novel zeolite phase denoted SSZ-35 over the entire lattice substitution range from fairly aluminum rich (SAR = 30)[21] to pure silica. The diffraction pattern of SSZ-35 is presented in Figure 2. The strong nonbonded SDA/zeolite interaction energy between entry **29** and SSZ-35 accounts for the high phase selectivity (as will be discussed in more detail in Section 3); replacing just one *N*-methyl group with ethyl prevents the crystallization of SSZ-35. Entry **29** successfully achieves the design goals for generating new zeolite topologies and provides an example of the fifth domain of zeolite formation, in which strong nonbonded SDA/

zeolite interactions stabilize a particular zeolite structure over a wide range of lattice substitution.

The extensions of methyl groups off the bicyclic ring system of entry **9** (Table 2) also creates a bulky spheriodal SDA that satisfies the design strategy; however, the phase specificity in this case is much weaker than that in the previous case. The use of organocation **9** (Table 2) in zeolite synthesis reactions with silica-to-alumina ratios (SAR) of 100 also results in the formation of SSZ-35 (entry **9**, Table 4). Increasing the alumina or borate content in zeolite synthesis reactions containing entry **9** (Table 2) results in the novel zeolitic phase denoted SSZ-36 (entry **9**, Table 4). A diffraction pattern for SSZ-36 is shown in Figure 3a. Clearly, entry **9** has a weaker selectivity for SSZ-35 than entry **29** and illustrates the competing influences of the kinetic control of the inorganic gel composition with the

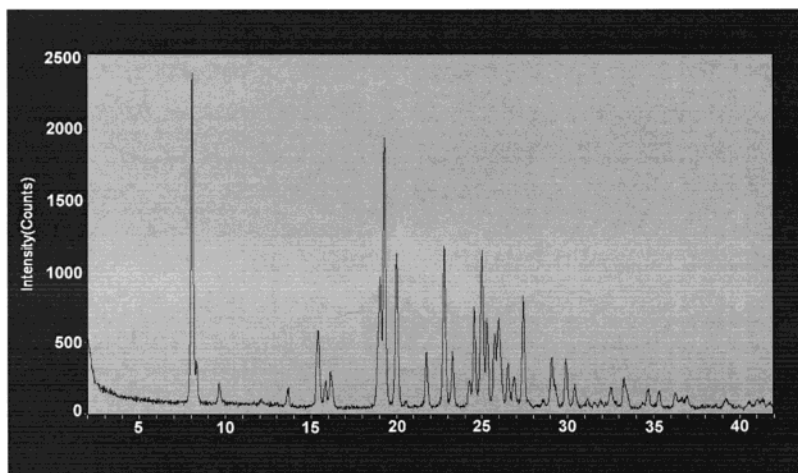(21) Zones, S. I.; Nakagawa, Y. U.S. Patent 5,785,947, 1998.

Figure 2. X-ray powder diffraction pattern for SSZ-35.
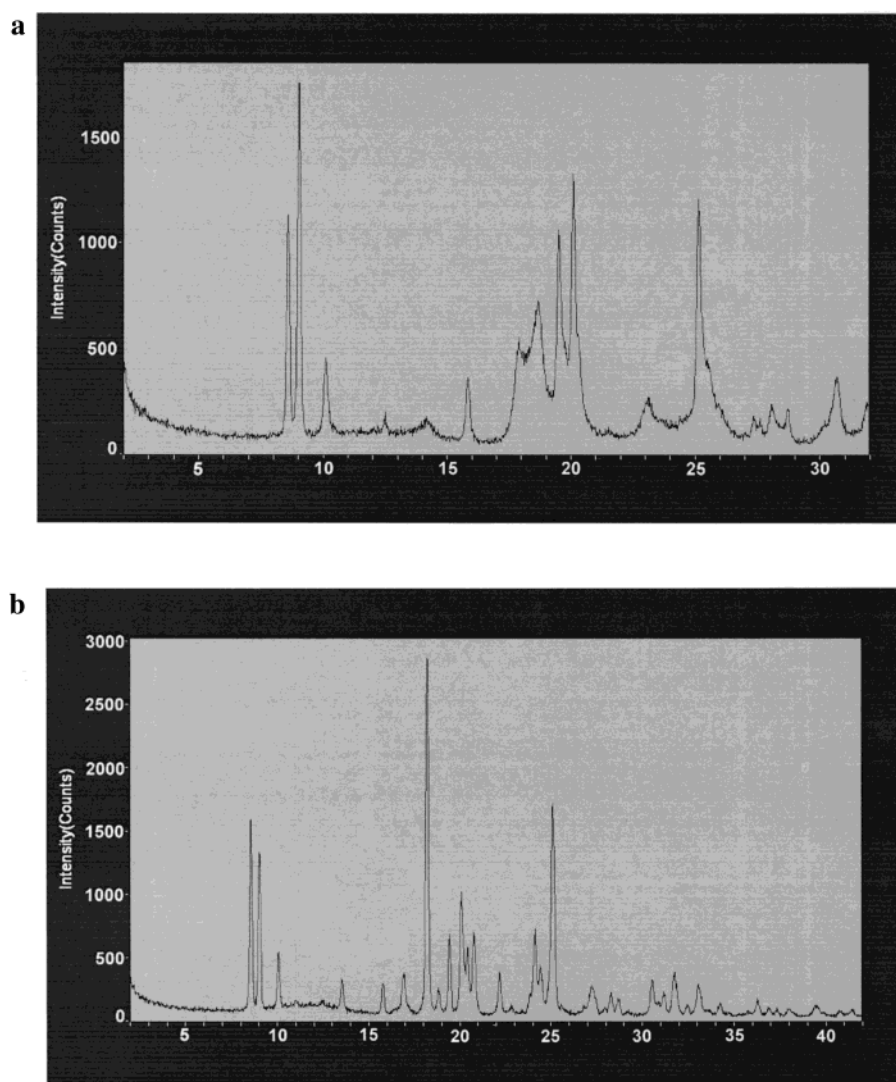
Figure 3. Two examples of X-ray powder diffraction patterns for SSZ-36: (a) from a synthesis using entry **9** and (b) from entry **18**.

thermodynamic influences of the organic/inorganic interactions in the zeolite formation, and this will be explored more thoroughly in Section 3.

b. Summary of SSZ-35, SSZ-36, and SSZ-39 Syntheses. A number of zeolite synthesis trends are apparent within the group of 37 organocation guest molecules employed in this study (Table 4). The SSZ-36 material is generally favored by the mono- and bicyclic ring systems (Tables 1 and 2) with ring methylation beyond the charged nitrogen and tends to preferentially form at higher heteroatom lattice substitutions; no pure silica example has been found. The SSZ-36 product can be crystallized at high lattice substitution with SAR $= 10-40$[21] and can also be crystallized in the presence of a number of guest molecules when the synthesis conditions are rich in borate. It

Figure 4. Framework representation of SSZ-35 showing the 10-ring portals leading into larger cavities.

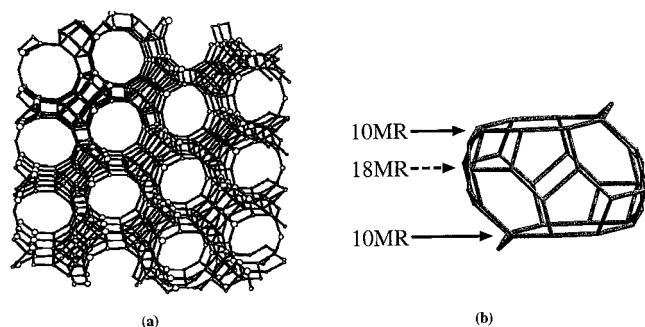is important to note that certain reflection intensities and breadths observed in the SSZ-36 powder X-ray diffraction data depend on the degree of lattice substitution and the organocation employed in the SSZ-36 syntheses. Such preferential line broadening in the powder X-ray data is indicative of faulting and will be discussed in greater detail below in the context of the SSZ-36 structure.

SSZ-35 is most effectively crystallized in the presence of tri- and tetracyclic charged compounds (Table 3) with no additional ring derivatization and tends to be favored at low lattice substitution. The calculated SDA/zeolite interaction energy indicates that the tri- and tetracyclic quaternized amine molecules provide favorable van der Waals stabilization of the SSZ-35 cages, as will be discussed in more detail in Section 3. The distinct preference for forming this new zeolite structure via the tri- and tetracyclic organocations indicates that not only the overall size of the molecule but also the shape of the molecule are important in considering new molecules as SDAs for zeolite synthesis. Conspicuously absent in these results are SDA candidates with pendant Me_3N^+ groups. Only entry **10**, in one particular reaction, produces SSZ-36. To date, there are no examples of these kinds of SDAs crystallizing SSZ-35.

As discussed previously, SSZ-39 is able to be crystallized from a wide range of the SDA molecules in Tables 1−3 at very high lattice substitution. The reactions employing high alumina content also require a high hydroxide concentration in order to solubilize the alumina and tend to result in cage-based zeolites with small portals such as SSZ-39 due to the ordering of aluminum in the framework; the details of the SSZ-39 structure are presented below. Highly lattice substituted even-membered-ring-containing zeolites such as CHA and SSZ-39 tend to be observed when the inorganic gel composition predominates over the organic/inorganic interactions.

2. Zeolite Structures. a. SSZ-35. The details of the structure solution of the high-silica, molecular sieve SSZ-35 are described in a recent publication.[22] The structure contains an unusual, one-dimensional channel system with pore openings that alternate between rings containing 10 tetrahedral atoms (T-atoms) and 18 tetrahedral atoms (Figure 4a). This alternating pore diameter can also be viewed as arising from the stacking of $[4^4 5^8 6^6 10^2]$ cages with 10 T-atom openings at the top and bottom of the cages (Figure 4b).

b. SSZ-39. The refined[17] unit cell parameters for SSZ-39 obtained from the synchrotron powder XRD data are $a =$ 13.629692 Å, $b = 12.674772$ Å, $c = 18.473045$ Å, and $\beta =$ 89.9288°. Analysis of the systematic absences for the monoclinic

structure indicates a space group assignment consistent with $C2/c$ (No. 15). The structure solution of the new aluminosilicate SSZ-39 is obtained by the isomorphic substitution of the non-oxygen framework atoms in the SAPO-18 structure[23] with silicon atoms.

For the Rietveld refinements of SSZ-39 from the synchrotron powder XRD data (SPXRD), 10 background parameters (shifted Chebychev function), the scale factor, and the zero shift were first refined, followed by the refinement of the lattice parameters, six profile parameters (Simpson's rule integration of the pseudo-Voight function), and finally, the atomic positions and the isotropic temperature factors for all the atoms were refined.

Ninety-four variables were refined in the final Rietveld refinement over a profile range of 2.0−50.0° ($l = 1.20106$ Å, step sizes $= 0.005°$, resulting in 9600 observables) containing 649 reflections. Fifty-seven soft constraints were employed (24, $d(Si-O) = 1.61(01)$ Å; 33, $d(O-O) = 2.61$ Å), resulting in an average $d(Si-O)$ of 1.611 Å with a maximum of 1.644 Å and minimum of 1.588 Å (minimum of 105.5°), and the average Si−O−Si angle being 148.57° with a maximum of 152.6° dimension and a minimum of 141.3°. The final residual values were $wR_p = 11.338\%$ and $R_p = 9.30\%$. The Fourier difference map showed maximum peak heights all less than 0.5 e$^-$/Å. The refinement data are presented in Figure 5. The atomic position together with the isotropic temperature factors are presented in the Supporting Information.

The structure of SSZ-39 is composed of columns of double six-ring units that stack along the [001] direction (Figure 6a). These columns interconnect through bridging oxygen atoms to form layers that connect through other oxygen atoms (Figure 6b). The layerlike units stack along the [010] direction and are related through mirror planes (Figure 6c). This layer stacking of the sheets of double six-ring units gives rise to a cage system similar in volume to the cages found in the SSZ-35 structure. They are interconnected in three dimensions by eight-ring unitss as shown in Figure 6d and e.

c. SSZ-36. Twin faulting and intergrowth occurs frequently in zeolitic materials due in part to the poor specificity of the structure-directing agent for a particular end-member polymorph of the fault series. Twin faulting in zeolites is commonly manifested as a stacking disorder of a layerlike unit in which the successively stacked layers can be related through either mirror planes or inversion centers. As the density of the twin faults increases, i.e., the distance between the twin faults decrease, broadening or streaking of reflection intensities in the diffraction data occurs.

As seen in Figure 3a, the SSZ-36 material synthesized from entry **9** in Table 2 contains a distribution of reflection widths that, together with SEMs showing uniform crystal morphology, indicate that the crystals contain a high density of twin faults. The reflections at smaller scattering angles lack significant broadening in comparison to the reflections near 18° 2θ. These sharp reflections resemble the low scattering angle portion of the powder X-ray diffraction pattern observed for the RUB-13 material (RTH).[24]

The RTH topology possesses a two-dimensional pore system circumscribed by eight-membered rings and contains large cages that are interconnected through the eight-membered rings. The RUB-13 structure can be viewed as resulting from the stacking of layerlike units related through mirror planes that can twin parallel to c*.[24] This twin fault gives rise to layerlike units that

(22) (a) Wagner, P.; Medrud, R. C.; Davis, M. E.; Zones, S. I. Proceedings of the 12th International Zeolite Conference, Baltimore, MD, July 1998; Recent Progress Reports Poster Abstract, RR. (b) Wagner, P.; Medrud, R. C.; Davis, M. E.; Zones, S. I. *Angew. Chem., Int. Ed.* **1999**, *38*, 1269−1272.

(23) Simmen, A.; McCusker, L. B.; Baerlocher, Ch.; Meier, W. M. *Zeolites* **1991**, *11*, 654.
(24) Vortman, S.; Marler, B.; Gies, H.; Daniels, P. *Microporous Mater.* **1995**, *4*, 111.
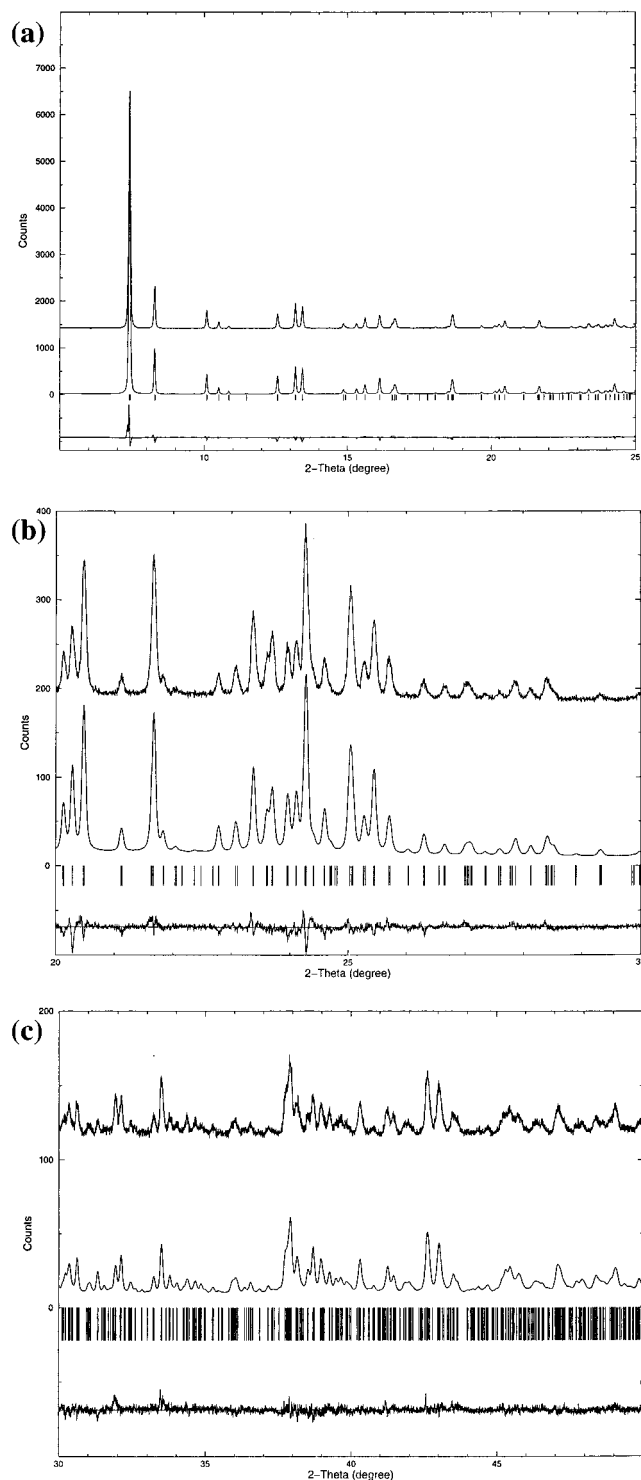
(a)

(b)

(c)

Figure 5. Calculated and experimental (synchrotron data) diffraction patterns for SSZ-39.

are related through inversion centers and results in the formation of a new large cage structure that differs in shape from the cages found in the RUB-13 structure but that possesses a similar volume. The synthesis and structure solution of this other material has recently been reported[25] and has been given the IZC code ITE. Figure 7 (adapted from ref 25) shows the comparison of the symmetry differences for the two cage types generated for these two end-member structures. The representation shows the two-dimensional eight-ring pores system that intersects into sizable cages.

(25) Camblor, M. A.; Corma, A.; Lightfoot, P.; Villaescusa, L. A.; Wright, P., A. *Angew. Chem., Int. Ed.* **1997**, *36*, 2659.
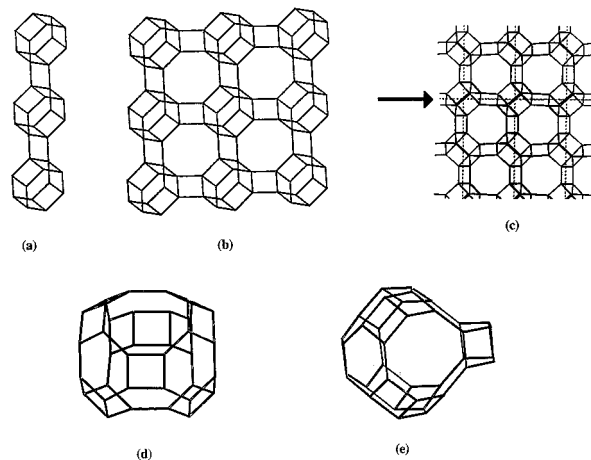

Figure 6. Linkages for the chains and connectivities used to construct the cavities in SSZ-39. See the text for greater discussion.

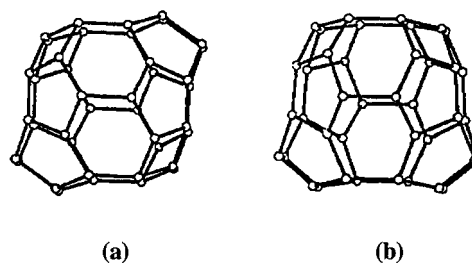
(a)   **(b)**

Figure 7. Comparison of the cage constructions for ITE and RTH (left). It can be seen that a difference of one symmetry operator results in the two unique structures (taken from ref 25).
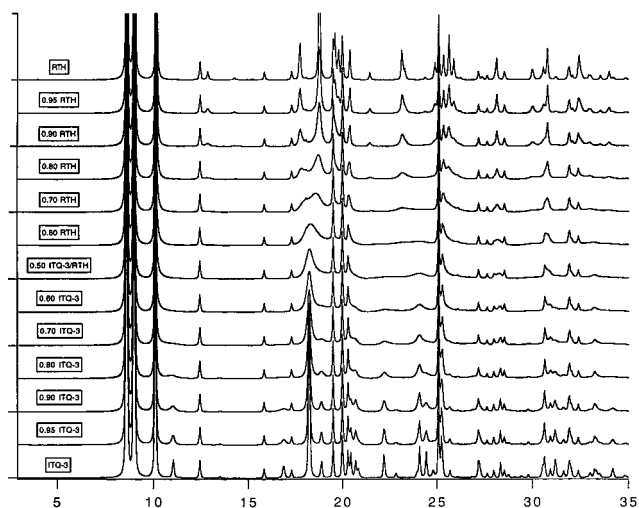

Figure 8. DIFFaX analysis for simulation of polymorph intergrowth from end members ITE and RTH.

Simulations of powder X-ray diffraction (PXRD) data for crystals containing varying RTH−ITE twin fault densities were performed using DiFFaX[26] (Figure 8). At the low twin fault densities, the PXRD data closely match the PXRD data resulting from the pure end-member polymorph; however, as the twin fault density increases, broad reflection intensities arise due to the decreasing distance between the twin faults, as previously discussed.

SSZ-36 has been synthesized from a number of different organic structure-directing agents, and depending on the particular SDA and the degree of heteroatom substitution, the

(26) Treacy, M. M. J.; Deem, M. W.; Newsam, J. M. DIFFaX Version 1.801, 1995.
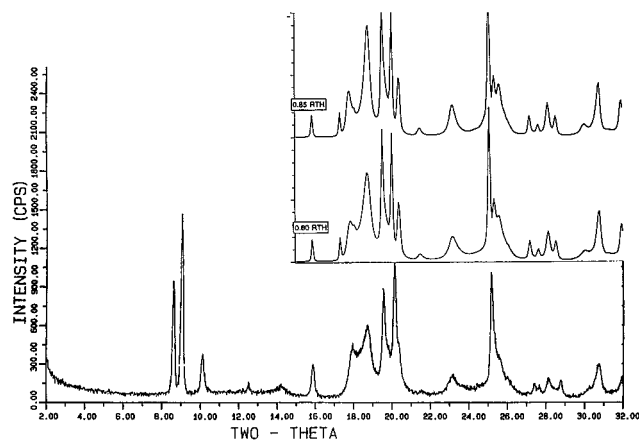
Figure 9. Comparison of the experimental XRD powder data from Figure 3a and the DIFFaX modeling of polymorph mixtures in the range of RTH having 80% probability.

PXRD data are affected to varying degrees by twin faulting between the RUB-13 and the ITQ-3 structures. For example, comparison of the experimental powder X-ray diffraction pattern of SSZ-36 synthesized from entry **9**, Table 2 (Figure 3a), to the fault simulations indicates that this material is a faulted intermediate between the RTH and the ITE structures with a fault probability of approximately 80% RTH (Figure 9). In contrast, Figure 3b shows the powder X-ray diffraction pattern that results from the use of entry **18** in Table 2. Comparison of these PXRD data with the fault simulations in Figure 8 indicates that the material is nearly fault-free. The PXRD pattern is characteristic of a material consisting predominantly of the structure of the pure end-member polymorph ITQ-3. The product here is not pure silica, as is the case for the published ITE.

3. Correlations between Guest Molecules and Phase Selectivities. Here, we present several molecular modeling studies in which the nonbonded SDA/zeolite energy of interaction is correlated with the observed zeolite phase selectivity from a particular SDA. These results provide insights into the factors that affect the specificity for the observed zeolite phases from the designed SDA molecules.

As mentioned in the Discussion section, the SSZ-36 material is favored by the mono- and bicyclic ring systems with ring methylation beyond the charged nitrogen (Table 4). The SDAs that possess ring methylation beyond the charged nitrogen show a strong selectivity for SSZ-36 over SSZ-35. Entries **19** and **20** (Table 2) present an interesting example of this phenomenon, in which the addition of one methyl group to the carbon ring of the [4.1.1] octane molecule (entry **19**) dramatically shifts the phase selectivity from SSZ-35 to SSZ-36. (A similar comparison can be made for **14** vs **17**.) Molecular modeling calculations were employed in order to gain a better understanding of the strong specificity of the [4.1.1] octane molecule with and without the ring methyl group. The calculated nonbonded energy of the entry **20**/SSZ-35 interaction indicates that entry **20** strongly stabilizes the SSZ-35 cage structure (−11.81 kcal/cage). However, the addition of the methyl group to the carbon ring (entry **19**) results in a positive energy of interaction (0.69 kcal/cage), indicating that the molecule is too large to fit into the cages of the SSZ-35 material. The modeling calculations suggest that the mono- and bicyclic ring SDA molecules with ring methylation beyond the charged nitrogen are either too large or of the wrong shape to fit within the cages of the competing SSZ-35 phase. These results support the design strategy outlined in the Introduction for developing rigid molecules that are too large to fit into the cage or pore system of competing phases.

Table 5. Stabilization Energy for Compound **29** (Table 3) in the Cages of the Competing Zeolite Phases

zeolite	compound **29**, kcal/cage
ITE	−19.9
RTH	−18.8591
SSZ-39	−6.79554
SSZ-35	−20.87

As discussed previously, the SSZ-36 material that results from entry **9** is a faulted intermediate between the RTH and the ITE structures. To gain a better understanding of the effects of the SDA molecule on zeolite faulting, entry **9** was modeled in the cages of both ITE and RTH. The resulting VDW energies of stabilization for **9** in the RTH cages is −14.9 kcal/cage, while the stabilization energy of **9** in the ITE cages is −14.03 kcal/cage. The similarities of the nonbonded van der Waals energy of stabilization for entry **9** within both the ITE and RTH cages suggest that this compound may lead to a structure that is a faulted intermediate between the RTH and ITE structures. The experimentally observed powder X-ray data for the SSZ-36 material that results from entry **9** reveals that it is faulted and possesses a fault probability toward the RTH structure of approximately 80% (Figure 9).

Additional insight into the phase selectivity of the organic guests for a particular silicate framework is gained by examining the behavior of the tri- and tetracyclic molecules in Table 3. With the lone exception of entry **37**, these guest molecules all produce SSZ-35. These molecules must therefore possess the correct size and geometry to stabilize the SSZ-35 cages.

An interesting case of SSZ-35 phase selectivity is observed for the tetracyclic entry **29**, which crystallizes SSZ-35 over the entire lattice substitution range. Molecular modeling was employed to determine the effects of the van der Waals (VDW) energy of interaction between entry **29** and the cages of the SSZ-35 phase and the cages of the competing phases (ITQ-3, RUB-13, and SSZ-39). The calculation results are given in Table 5 and indicate that entry **29** strongly stabilizes SSZ-35 relative to these competing phases. The significant stabilization of SSZ-35 over SSZ-39 (−20.87 vs −6.79 kcal/cage) is particularly interesting. This result is consistent with the experimental observation that, even at high aluminum substitution, entry **29** stabilizes the SSZ-35 structure over the six-ring-rich structures that commonly result from syntheses containing high alumina content and high OH/Si ratios (entry **29**, Table 4, SAR = 30).

Conclusions

Here, we have presented the results of the design strategy for organic structure-directing agents that lead to three novel zeolite phases: SSZ-35, SSZ-36, and SSZ-39. The strategy involves synthesizing rigid bulky organocations that are too large or of the wrong geometry to fit into the cavities or pores of commonly encountered competing phases such as the clathrates or the straight one-dimensional channel system zeolites, e.g., SSZ-31 and MTW.

The tri- and tetracyclic charged compounds with no additional ring derivatization (Table 3) are found to be very effective structure-directing agents for the novel zeolitic phase, SSZ-35. This new material also tends to be favored at low lattice substitution. The molecular modeling results indicate that the tri- and tetracyclic quaternized amine molecules are particularly effective in stabilizing the SSZ-35 cages. The structure of SSZ-35 contains an unusual, one-dimensional channel system containing an alternating 10- and 18-MR pore diameter that can also be viewed as arising from the stacking of cages with 10 T-atom openings at the top and bottom of the cages.

The novel zeolitic phase, SSZ-36, is favored by the mono- and bicyclic SDA molecules in Tables 1 and 2 that possess ring methylation beyond the nitrogen. Molecular modeling results indicate that these molecules are typically too large or are of the wrong geometry to fit within the cages of potentially competing phases such as SSZ-35. The SSZ-36 phase also tends to be favored at higher lattice substitutions; no all-silica SSZ-36 materials were synthesized. The structure of SSZ-36 is found to be a faulted intermediate between the two end-member polymorphs RTH and ITE, that possess two-dimensional pore systems circumscribed by eight-membered rings and that intersect into large cavities.

The SSZ-39 material is a frequently observed product of the high-alumina-containing syntheses (SAR = 30) using the organic molecules in Tables 1−3. If the inorganic gel composition predominates over the organic/inorganic interactions in the high-alumina-containing zeolite synthesis, then cage-based zeolites containing even-membered ring constructions and small portals such as SSZ-39 tend to form. The structure of SSZ-39 was found to be isomorphous with the aluminophosphate molecular sieve, SAPO-18 (AEI).

The successful strategy of designing organic zeolite directing molecules that are too large or of the wrong geometry to stabilize commonly encountered competing phases in order to synthesize novel zeolite materials is complemented by the computational modeling results that provide useful insights into the observed zeolite phase selectivities of the designed SDA molecules. Understanding the effects of the nonbonded energy of the organic SDA/zeolite interaction on zeolite phase selectivity and fault probability will play a fundamental role in the future discovery of new zeolite phases through rational SDA design.

Supporting Information Available: Details of the syntheses of the organocations **1−37** and relevant references, and a table of atomic positions and isotropic temperature factors for SSZ-39 (PDF). This material is available free of charge via the Internet at http://pubs.acs.org.

JA990722U